

A computational model of human auditory signal processing and perception

Jepsen, Morten Løve; Ewert, Stephan D.; Dau, Torsten

Published in:
Journal of the Acoustical Society of America

Link to article, DOI:
[10.1121/1.2924135](https://doi.org/10.1121/1.2924135)

Publication date:
2008

Document Version
Publisher's PDF, also known as Version of record

[Link back to DTU Orbit](#)

Citation (APA):
Jepsen, M. L., Ewert, S. D., & Dau, T. (2008). A computational model of human auditory signal processing and perception. *Journal of the Acoustical Society of America*, 124(1), 422-438. DOI: 10.1121/1.2924135

DTU Library

Technical Information Center of Denmark

General rights

Copyright and moral rights for the publications made accessible in the public portal are retained by the authors and/or other copyright owners and it is a condition of accessing publications that users recognise and abide by the legal requirements associated with these rights.

- Users may download and print one copy of any publication from the public portal for the purpose of private study or research.
- You may not further distribute the material or use it for any profit-making activity or commercial gain
- You may freely distribute the URL identifying the publication in the public portal

If you believe that this document breaches copyright please contact us providing details, and we will remove access to the work immediately and investigate your claim.

A computational model of human auditory signal processing and perception

Morten L. Jepsen

Centre for Applied Hearing Research, Acoustic Technology, Department of Electrical Engineering, Technical University of Denmark, DK-2800 Kgs. Lyngby, Denmark

Stephan D. Ewert

Medizinische Physik, Carl von Ossietzky Universität Oldenburg, D-26111 Oldenburg, Germany

Torsten Dau^{a)}

Centre for Applied Hearing Research, Acoustic Technology, Department of Electrical Engineering, Technical University of Denmark, DK-2800 Kgs. Lyngby, Denmark

(Received 2 August 2007; revised 31 March 2008; accepted 17 April 2008)

A model of computational auditory signal-processing and perception that accounts for various aspects of simultaneous and nonsimultaneous masking in human listeners is presented. The model is based on the modulation filterbank model described by Dau *et al.* [J. Acoust. Soc. Am. **102**, 2892 (1997)] but includes major changes at the peripheral and more central stages of processing. The model contains outer- and middle-ear transformations, a nonlinear basilar-membrane processing stage, a hair-cell transduction stage, a squaring expansion, an adaptation stage, a 150-Hz lowpass modulation filter, a bandpass modulation filterbank, a constant-variance internal noise, and an optimal detector stage. The model was evaluated in experimental conditions that reflect, to a different degree, effects of compression as well as spectral and temporal resolution in auditory processing. The experiments include intensity discrimination with pure tones and broadband noise, tone-in-noise detection, spectral masking with narrow-band signals and maskers, forward masking with tone signals and tone or noise maskers, and amplitude-modulation detection with narrow- and wideband noise carriers. The model can account for most of the key properties of the data and is more powerful than the original model. The model might be useful as a front end in technical applications. © 2008 Acoustical Society of America. [DOI: 10.1121/1.2924135]

PACS number(s): 43.66.Ba, 43.66.Dc, 43.66.Fe [BCM]

Pages: 422–438

I. INTRODUCTION

There are at least two reasons why auditory processing models are constructed: to represent the results from a variety of experiments within one framework and to explain the functioning of the system. Specifically, processing models help generate hypotheses that can be explicitly stated and quantitatively tested for complex systems. Models of auditory processing may be roughly classified into biophysical, physiological, mathematical (or statistical), and perceptual models depending on which aspects of processing are considered. Most of the models can be broadly referred to as functional models, that is, they simulate the experimentally observed input-output behavior of the auditory system without explicitly modeling the precise internal biophysical mechanisms involved.

The present study deals with the modeling of perceptual masking phenomena, focusing on effects of intensity discrimination and spectral and temporal masking. Explaining basic auditory masking phenomena in terms of physiological mechanisms has a long tradition. There have been systematic attempts at predicting psychophysical performance limits from the activity of auditory nerve (AN) fibers (e.g., Siebert,

1965, 1970; Heinz *et al.*, 2001a, 2001b, Colburn *et al.*, 2003), combining analytical and computational population models of the AN with statistical decision theory. A general result has been that those models that make optimal use of all available information from the AN (e.g., average rate, synchrony, and nonlinear phase information) typically predict performance that is one to two orders of magnitude better than human performance, while the trends often match well human performance.

Other types of auditory masking models are to a lesser extent inspired by neurophysiological findings and make certain simplifying assumptions about the auditory processing stages. Such an “effective” modeling strategy does not allow conclusions about the details of signal processing at a neuronal level. On the other hand, if the effective model accounts for a variety of data, this suggests certain general processing principles. These, in turn, may motivate the search for neural circuits in corresponding physiological studies. Models of temporal processing typically consist of an initial stage of bandpass filtering, reflecting a simplified action of basilar-membrane (BM) filtering. Each filter is followed by a nonlinear device. In recent models, the nonlinear device typically includes two processes, half-wave rectification and a compressive nonlinearity, resembling the compressive input-output function on the BM (e.g., Ruggero and Rich, 1991; Oxenham and Moore, 1994; Oxenham *et al.*,

^{a)}Author to whom correspondence should be addressed. Electronic mail: tda@elektro.dtu.dk

1997; Plack and Oxenham, 1998; Plack *et al.*, 2002). The output is fed to a smoothing device implemented as a low-pass filter (Viemeister, 1979) or a sliding temporal integrator (e.g., Moore *et al.*, 1988). This is followed by a decision device, typically modeled as the signal-to-noise ratio. Forward and backward masking have been accounted for in terms of the build-up and decay processes at the output of the sliding temporal integrator. The same model structure has also been suggested to account for other phenomena associated with temporal resolution, such as gap detection and modulation detection (e.g., Viemeister, 1979).

An alternative way of describing forward masking is in terms of neural adaptation (e.g., Jesteadt *et al.*, 1982; Nelson and Swain, 1996; Oxenham, 2001; Meddis and O'Mard, 2005). A few processing models include adaptation and account for several aspects of forward masking (e.g., Dau *et al.*, 1996a, 1996b; Buchholz and Mourjoloulus, 2004a, 2004b; Meddis and O'Mard, 2005). It appears that the two types of models, temporal integration and adaptation, can lead to similar results even though they seem conceptually different (Oxenham, 2001; Ewert *et al.*, 2007).

Dau *et al.* (1996a) proposed a model to account for various aspects of simultaneous and nonsimultaneous masking using one framework. The model includes a linear, one-dimensional transmission-line model to simulate BM filtering (Strube, 1985), an inner-hair-cell transduction stage, an adaptation stage (Püschel, 1988), and an 8-Hz modulation lowpass filter, corresponding to an integration time constant of 20 ms. The adaptation stage in that model is realized by a chain of five simple nonlinear circuits, or feedback loops (Püschel, 1988; Dau *et al.*, 1996a). An internal noise is added to the output of the preprocessing that limits the resolution of the model. Finally, an optimal detector is attached that acts as a matched-filtering process. An important general feature of the model of Dau *et al.* (1996a) is that, once it is calibrated using a simple intensity discrimination task to adjust its internal-noise variance, it is able to quantitatively predict data from other psychoacoustic experiments without further fitting. Part of this flexibility is caused by the use of the matched filter in the decision process. The optimal detector automatically “adapts” to the current task and is based on the cross correlation of a template, a suprathreshold representation of the signal to be detected in a given task, with the internal signal representation at the actual signal level.

In a subsequent modeling study (Dau *et al.*, 1997a, 1997b), the gammatone filterbank model of Patterson *et al.* (1995) was used instead of Strube's transmission-line implementation because its algorithm is more efficient and the bandwidths matched estimates of auditory-filter bandwidths more closely. The modulation lowpass filter was replaced by a modulation filterbank, which enables the model to reflect the auditory system's high sensitivity to fluctuating sounds and to account for amplitude-modulation (AM) detection and masking data (e.g., Bacon and Grantham, 1989; Houtgast, 1989; Dau *et al.*, 1997a; Verhey *et al.*, 1999; Piechowiak *et al.*, 2007). The modulation filterbank realizes a limited-resolution decomposition of the temporal modulations and was inspired by neurophysiological findings in the auditory brainstem (e.g., Langner and Schreiner, 1988; Palmer, 1995).

The parameters of the filterbank were fitted to perceptual modulation masking data and are not directly related to the parameters from physiological models that describe the transformation from a temporal neural code into a rate-based representation of AM in the auditory brainstem (Langner, 1981; Hewitt and Meddis, 1994; Nelson and Carney, 2004; Dicke *et al.*, 2007).

The preprocessing of the model described by Dau *et al.* (1996a, 1997a) has been used in a variety of applications, e.g., for assessing speech quality (Hansen and Kollmeier, 1999, 2000), for predicting speech intelligibility (Holube and Kollmeier, 1996), as a front-end for automatic speech recognition (Tchorz and Kollmeier, 1999), for objective assessment of audio quality (Huber and Kollmeier, 2006), and for signal-processing distortion (Plasberg and Kleijn, 2007). The model has also been extended to predict binaural signal detection (Breebaart *et al.*, 2001a, 2001b, 2001c) and across-channel monaural processing (Piechowiak *et al.*, 2007).

However, despite some success with the model of Dau *et al.* (1997a), there are major conceptual limitations of the approach. One of these is that the model does not account for nonlinearities associated with BM processing since it uses the (linear) gammatone filterbank (Patterson *et al.*, 1995). Thus, for example, the model must fail in conditions which reflect level-dependent frequency selectivity, such as in spectral masking patterns. Also, even though the model includes effects of adaptation which account for certain aspects of forward masking, it must fail in those conditions that directly reflect the nonlinear transformation on the BM. This, in turn, implies that the model will not be able to account for consequences of sensorineural hearing impairment for signal detection since a realistic cochlear representation of the stimuli in the normal system is missing as a reference.

Implementing a nonlinear BM processing stage in the framework of the model is a major issue since the interaction with the successive static and dynamic processing stages can strongly affect the internal representation of the stimuli at the output of the preprocessing depending on the particular experimental condition. For example, how does the level-dependent cochlear compression affect the results in conditions of intensity discrimination? To what extent are the dynamic properties of the adaptation stage affected by the fast-acting cochlear compression? What is the influence of the compressive peripheral processing on the transformation of modulations in the model? In more general terms, the question is whether a modified model that includes a realistic (but more complex) cochlear stage can *extend* the predictive power of the original model. If this cannot be achieved, major conceptual changes of the modeling approach would most likely be required.

In an earlier study (Derleth *et al.*, 2001), it was suggested how the model of Dau *et al.* (1997a, 1997b), referred to in the following as the “original model,” could be modified to include fast-acting compression, as found in BM processing. Different implementations of fast-acting compression were tested either through modifications of the adaptation stage or by using modified, level-dependent gammatone filters (Carney, 1993). Derleth *et al.* (2001) found that the temporal-adaptive properties of the model were

strongly affected in all implementations of fast-acting compression; their modified model thus failed in conditions of forward masking. It was concluded that, in the given framework, the model would only be able to account for the data when an expansion stage after BM compression was assumed (which would then partly compensate for cochlear compression). However, corresponding explicit predictions were not generated in their study.

Several models of cochlear processing have been developed recently (e.g., Heinz *et al.*, 2001b; Meddis *et al.*, 2001; Zhang *et al.*, 2001; Bruce *et al.*, 2003; Irino and Patterson, 2006) which differ in the way that they account for the nonlinearities in the peripheral transduction process. In the present study, the dual-resonance nonlinear (DRNL) filterbank described by Meddis *et al.* (2001) was used as the peripheral BM filtering stage in the model—instead of the gammatone filterbank. In principle, any of the above cochlear models could instead have been integrated in the present modeling framework. The DRNL was chosen since it represents a computationally efficient and relatively simple functional model of peripheral processing. It can account for several important properties of BM processing, such as frequency- and level-dependent compression and auditory filter shape in animals (Meddis *et al.*, 2001). The DRNL structure and parameters were adopted to develop a human cochlear filterbank model by Lopez-Poveda and Meddis (2001) on the basis of pulsation-threshold data.

In addition to the changes at the BM level, several other substantial changes in the processing stages of the original model were made. The motivation was to incorporate findings from other successful modeling studies in the present framework. Models of human outer- and middle-ear transformations were included in the current model, none of which were considered in the original model. An expansion stage, realized as a squaring device, was assumed after BM processing, as in the temporal-window model (Plack and Oxenham, 1998; Plack *et al.*, 2002). Also, certain aspects of modulation processing were modified in the processing, motivated by recent studies on modulation detection and masking (Ewert and Dau, 2000; Kohlrausch *et al.*, 2000). The general structure of the original perception model, however, was kept the same.

The model developed in this study, referred to as the computational auditory signal-processing and perception (CASP) model in the following, was evaluated using a set of critical experiments, including intensity discrimination using tones and broadband noise, tone-in-noise detection as a function of the tone duration, spectral masking patterns with tone and narrow-band-noise signals and maskers, forward masking with noise and tone maskers, and AM detection with wide- and narrow-band-noise carriers. The experimental data from these conditions can only be accounted for if the compressive characteristics and the spectral and temporal properties of auditory processing are modeled appropriately.

Section II specifies the processing stages of the CASP model. Section III describes the experimental methods, the stimuli in the different conditions, and the parameters used in the simulations. Section IV focuses on the results of the ex-

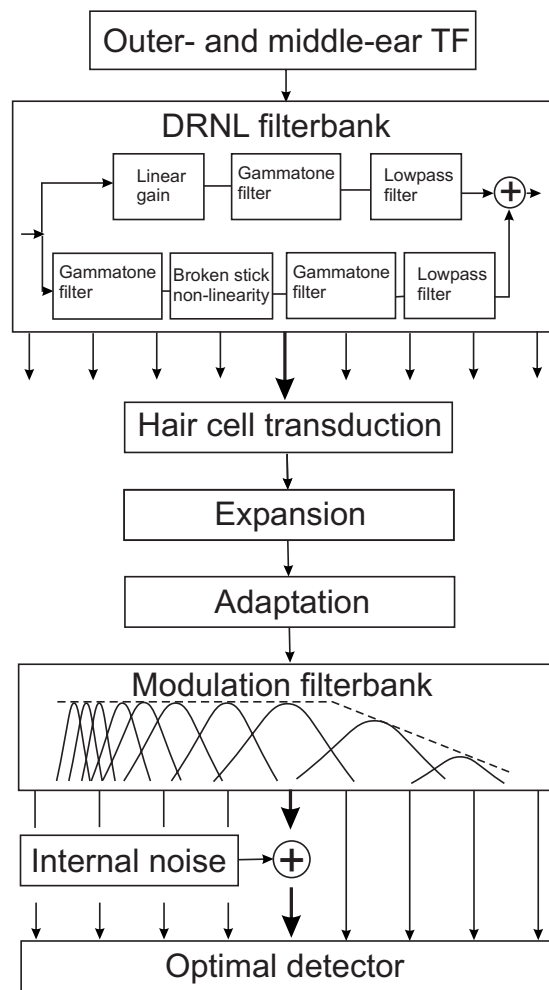


FIG. 1. Block diagram of the model structure. See text for a description of each stage.

periments and the corresponding simulations. The main outcomes of the study and perspectives for further modeling investigations are discussed in Sec. V.

II. DESCRIPTION OF THE MODEL

A. Overall structure

Figure 1 shows the structure of the CASP model.¹ The first stages represent the transformations through the outer and the middle ear, which were not considered by Dau *et al.* (1997a, 1997b). A major change to the original model was the implementation of the DRNL filterbank. The hair-cell transduction, i.e., the transformation from mechanical vibrations of the BM into inner-hair-cell receptor potentials, and the adaptation stage are the same as in the original model. However, a squaring expansion was introduced in the model after hair-cell transduction, reflecting the square-law behavior of rate-versus-level functions of the neural response in the AN (Yates *et al.*, 1990; Muller *et al.*, 1991). In terms of envelope processing, a first-order 150-Hz lowpass filter was introduced in the processing prior to the modulation band-pass filtering. This was done in order to limit sensitivity to fast envelope fluctuations, as observed in AM detection experiments with tonal carriers (Ewert and Dau, 2000; Kohl-

rausch *et al.*, 2000). The transfer functions of the modulation filters and the optimal detector are the same as used in the original model. The details of the processing stages are presented below (Sec. II B).

B. Processing stages in the model

1. Outer- and middle-ear transformations

The input to the model is a digital signal, where an amplitude of 1 corresponds to a maximum sound pressure level (SPL) of 100 dB. The amplitudes of the signal are scaled to be represented in pascals prior to the outer-ear filtering. The first stage of the auditory processing is the transformation through the outer and middle ears. As in the study of Lopez-Poveda and Meddis (2001), these transfer functions were realized by two linear-phase finite impulse response filters. The outer-ear filter was a headphone-to-eardrum transfer function for a specific pair of headphones (Pralong and Carlile, 1996). It was assumed that the headphone brand only has a minor influence as long as circumaural, open and diffuse-field equalized, quality headphones are considered, as was done in the present study. The middle-ear filter was derived from human cadaver data (Goode *et al.*, 1994) and simulates the mechanical impedance change from the outer ear to the middle ear. The outer- and middle-ear transfer functions correspond to those described by Lopez-Poveda and Meddis (2001, their Fig. 2). The combined function has a symmetric bandpass characteristic with a maximum at about 800 Hz and slopes of 20 dB/decade. The output of this stage is assumed to represent the peak velocity of vibration at the stapes as a function of frequency.

2. The DRNL filterbank

Meddis *et al.* (2001) developed an algorithm to mimic the complex nonlinear BM response behavior of physiological chinchilla and guinea pig observations. This algorithm includes two parallel bandpass processing paths, a linear one and a compressive nonlinear one, and its output represents the sum of the outputs of the two paths. The complete unit has been called the DRNL filter. The structure of the DRNL filter is illustrated in Fig. 1. The linear path consists of a linear gain function, a gammatone bandpass filter, and a low-pass filter. The nonlinear path consists of a gammatone filter, a compressive function which applies an instantaneous broken-stick nonlinearity, another gammatone filter, and, finally, a lowpass filter. The output of the linear path dominates the sum at high signal levels (above 70–80 dB SPL). The nonlinear path behaves linearly at low signal levels (below 30–40 dB SPL) and is compressive at medium levels (40–70 dB SPL). In the study of Meddis *et al.* (2001), the model parameters were fitted to physiological data so that the model accounted for a range of phenomena, including isoveLOCITY contours, input-output functions, phase responses, two-tone suppression, impulse responses, and distortion products. In a subsequent study, the DRNL filterbank was modified in order to simulate the properties of the human cochlea (Lopez-Poveda and Meddis, 2001) by fitting the model parameters to psychophysical pulsation-threshold data (Plack and Oxenham, 2000). These data have been assumed

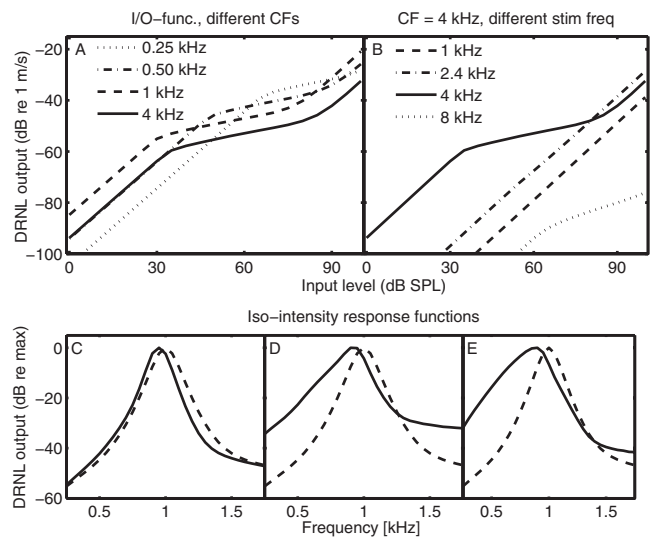


FIG. 2. Properties of the DRNL filterbank. Panel A shows the I/O functions for on-frequency stimulation at different CFs. Panel B shows the I/O functions for the filter with CF=4 kHz for tones with frequencies of 1, 2.4, 4, and 8 kHz. The solid curves in panels C, D, and E show the normalized magnitude transfer functions of the DRNL filter tuned to 1 kHz for input levels of 30, 60, and 90 dB SPL, respectively. The dashed curves indicate the transfer function of the corresponding fourth-order gammatone filter.

to estimate the amount of peripheral compression in human cochlear processing. The parameters of their model were estimated for different signal frequencies and Lopez-Poveda and Meddis (2001) suggested how to derive the parameters for a complete filterbank.

The CASP model includes the digital time-domain implementation of the DRNL filterbank described by Lopez-Poveda and Meddis (2001). However, slight changes in some of the parameters were made. The amount of compression was adjusted to stay constant above 1.5 kHz, whereas it was assumed to increase continuously in the original parameter set. This modification is consistent with recent findings of Lopez-Poveda *et al.* (2003) and Rosengard *et al.* (2005), where a constant amount of compression was estimated at signal frequencies of 2 and 4 kHz based on forward-masking experiments. A table containing the parameters that were modified is given in the Appendix. For implementation details, the reader is referred to Lopez-Poveda and Meddis (2001).

Some of the key properties of the implemented DRNL filter are reflected in the input/output (I/O) functions at different characteristic frequencies (CFs). Figure 2(A) shows I/O functions of the filters at 0.25, 0.5, 1, and 4 kHz. The 0.25 kHz function (dotted curve) is linear up to an input level of 60 dB SPL and becomes compressive at the highest levels. With increasing CFs, the level at which compression begins to occur decreases. It is well known that the compressive characteristics of the BM are most prominent near CF (0.2–0.5 dB/dB), at least for CFs above about 1 kHz, whereas the response is close to linear (0.8–1.0 dB/dB) for stimulation at frequencies well below CF (e.g., Ruggero *et al.*, 1997). Figure 2(B) shows the I/O functions for the filter centered at 4 kHz in response to tones with several input frequencies (1, 2.4, 4, 8 kHz). It can be seen that the largest response is generally produced by on-frequency

stimulation (4 kHz). The I/O functions for stimulation frequencies below CF are linear. The response to a tone with a frequency of one octave above CF (8 kHz) is compressive (dotted curve) but at a very low level.

Associated with the compressive transformation for on-frequency stimulation and the less compressive (close to linear) response to off-frequency stimulation is the level-dependent magnitude transfer function of the filter. The transfer function (normalized to the maximal tip gain) for the DRNL filter tuned to 1 kHz (solid curves) is shown for input levels of 30 dB SPL (panel C), 60 dB SPL (panel D), and 90 dB SPL (panel E). For comparison, the dashed curves indicate the transfer function of the fourth-order gammatone filter at the same CF. At the lowest level, 30 dB SPL, the transfer function of the DRNL is very similar to that of the gammatone filter. The bandwidth of the DRNL filter increases with level and the filter becomes increasingly asymmetric. With increasing level, the best frequency, i.e., the stimulus frequency that produces the strongest response, shifts toward lower frequencies, similar to physiological data from animals at higher frequencies (e.g., [Ruggero et al., 1997](#)). Behavioral data from [Moore and Glasberg \(2003\)](#) indicated that this shift may not occur at the 1-kHz site in humans. Nevertheless, the implementation as suggested by [Lopez-Poveda and Meddis \(2001\)](#) was kept in the present study. The output of the DRNL filterbank is a multi-channel representation, simulating the temporal output activity in various frequency channels. Each channel is processed independently in the following stages. The separation of center frequencies in the filterbank is one equivalent rectangular bandwidth, representing a measure of the critical bandwidth of the auditory filters as defined by [Glasberg and Moore \(1990\)](#).

3. Mechanical-to-neural transduction and adaptation

The hair-cell transduction stage in the model roughly simulates the transformation of the mechanical BM oscillations into receptor potentials. As in the original model, this transformation is modeled by half-wave rectification followed by a first-order lowpass filter ([Schroeder and Hall, 1974](#)) with a cutoff frequency of 1 kHz. The lowpass filtering preserves the temporal fine structure of the signal at low frequencies and extracts the envelope of the signal at high frequencies ([Palmer and Russell, 1986](#)). The output is then transformed into an intensity like representation by applying a squaring expansion. This step is motivated by physiological findings of [Yates et al. \(1990\)](#) and [Muller et al. \(1991\)](#) which provided evidence for a square-law behavior of rate-versus-level functions of AN fibers near the AN threshold (in guinea pigs).

The output of the squaring device serves as the input to the adaptation stage of the model which simulates adaptive properties of the auditory periphery. Adaptation refers to dynamic changes in the gain of the system in response to changes in input level. Adaptation has been found physiologically at the level of the AN (e.g., [Smith, 1977](#); [Westermann and Smith, 1984](#)). In the present model, the effect of adaptation is realized by a chain of five simple nonlinear circuits, or feedback loops, with different time constants as

described by [Püschel \(1988\)](#) and [Dau et al. \(1996a, 1997a\)](#). Each circuit consists of a lowpass filter and a division operation. The lowpass filtered output is fed back to the denominator of the divisor element. For a stationary input signal, each loop realizes a square-root compression. Such a single loop was first suggested by [Siebert \(1968\)](#) as a phenomenological model of AN adaptation. The output of the series of five loops approaches a logarithmic compression for stationary input signals. For input variations that are rapid compared to the time constants of the lowpass filters, the transformation through the adaptation loops is more linear, leading to an enhancement in fast temporal variations or onsets and offsets at the output of the adaptation loops. The time constants, ranging between 5 and 500 ms, were chosen to account for perceptual forward-masking data ([Dau et al., 1996a](#)). In response to signal onsets, the output of the adaptation loops is characterized by a pronounced overshoot. In the study by [Dau et al. \(1997a\)](#), this overshoot was limited, such that the maximum ratio of the onset response amplitude and steady-state response amplitude was 10. This version of the adaptation stage was also used in the CASP model.

4. Modulation processing

The output of the adaptation stage is processed by a first-order lowpass filter with a cutoff frequency at 150 Hz. This filter simulates a decreasing sensitivity to sinusoidal modulation as a function of modulation frequency ([Ewert and Dau, 2000](#); [Kohlrausch et al., 2000](#)). The lowpass filter is followed by a modulation filterbank. The highest modulation filter center frequencies in the filterbank are limited to one-quarter of the center frequency of the peripheral channel driving the filterbank and maximally to 1000 Hz, motivated by results from physiological recordings of [Langner and Schreiner \(1988\)](#) and [Langner \(1992\)](#). The lowest modulation filter is a second-order lowpass filter with a cutoff frequency of 2.5 Hz. The modulation filters tuned to 5 and 10 Hz have a constant bandwidth of 5 Hz. For modulation frequencies at and above 10 Hz, the modulation filter CFs are logarithmically scaled and the filters have a constant Q value of 2. The magnitude transfer functions of the filters overlap at their -3 dB points. As in the original model, the modulation filters are complex frequency-shifted first-order lowpass filters. These filters have a complex valued output and either the absolute value of the output or the real part can be considered. For the filters centered above 10 Hz, the absolute value is considered. This is comparable to the Hilbert envelope of the bandpass filtered output and only conveys information about the presence of modulation energy in the respective modulation band, i.e., the modulation phase information is strongly reduced. This is in line with the observation of decreasing monaural phase discrimination sensitivity for modulation frequencies above about 10 Hz ([Dau et al., 1996a](#); [Thompson and Dau, 2008](#)). For modulation filters centered at and below 10 Hz, the real part of the filter output is considered. In contrast to the original model, the output of modulation filters above 10 Hz was attenuated by a factor of $\sqrt{2}$, so that the rms value at the output is the same as for the low-frequency channels in response to a sinusoidal AM input signal of the same modulation depth.

5. The decision device

In order to simulate limited resolution, a Gaussian-distributed internal noise is added to each channel at the output of the modulation filterbank. The variance of the internal noise was the same for all peripheral channels and was adjusted so that the model predictions followed Weber's law in an intensity discrimination task. Specifically, predictions were fitted to intensity discrimination data of a 1 kHz pure tone at 60 dB SPL and of broadband noise at medium SPLs (see also Sec. IV A). The representation of the stimuli after the addition of the internal noise is referred to as the "internal representation." The decision device is realized as an optimal detector, as in the original model. Within the model, it is assumed that the subject is able to create a "template" of the signal to be detected. This template is calculated as the normalized difference between the internal representation of the masker plus a suprathreshold signal representation and that of the masker alone. The template is a three-dimensional pattern, with axes time, frequency, and modulation frequency. During the simulation procedure, the internal representation of the masker alone is calculated and subtracted from the internal representation in each interval of a given trial. Thus, in the signal interval, the difference contains the signal, embedded in internal noise, while the reference interval(s) contain internal noise only. For stochastic stimuli, the reference and signal intervals are affected both by internal noise and by the external variability of the stimuli. The (non-normalized) cross-correlation coefficient between the template and the difference representations is calculated, and a decision is made on the basis of the cross-correlation values obtained in the different intervals. The interval that produces the largest value is assumed to be the signal interval. This corresponds to a matched-filtering process (e.g., Green and Swets, 1966) and is described in more detail by Dau *et al.* (1996a).

III. EXPERIMENTAL METHOD

The experimental method, stimulus details, and simulation parameters are described below. In the present study, data were collected for tone-in-noise detection and forward masking, while the data on intensity discrimination, spectral masking, and modulation detection were taken from the literature (Houtsma *et al.*, 1980; Moore *et al.*, 1998; Dau *et al.*, 1997a; Viemeister, 1979).

A. Subjects

Four normal-hearing listeners, aged between 24 and 28 years, participated in the experiments. They had pure-tone thresholds of 10 dB hearing level or better for frequencies between 0.25 and 8 kHz. One subject was the first author and had experience with psychoacoustic experiments. The other three subjects had no prior experience in listening tests. These three subjects were paid for their participation on an hourly basis and received 30 min training sessions before each new experiment. There were no systematic improvements in thresholds during the course of the experiments. Measurement sessions ranged from 30 to 45 min depending

of the subject's ability to focus on the task. In all measurements, each subject completed at least three runs for each condition.

B. Apparatus and procedure

All stimuli were generated and presented using the AFC-Toolbox for MATLAB (Mathworks), developed at the University of Oldenburg, Germany, and the Technical University of Denmark. The sampling rate was 44.1 kHz and signals were presented through a personal computer with a high-end, 24 bit sound card (RME DIGI 96/8 PAD) and headphones (Sennheiser HD-580). The listeners were seated in a double-walled, sound insulated booth with a computer monitor, which displayed instructions and gave visual feedback.

A three-interval, three-alternative forced choice paradigm was used in conjunction with an adaptive 1-up-2-down tracking rule. This tracked the point on the psychometric function corresponding to 70.7% correct. The initial step size was 4 dB. After each second reversal, the step size was halved until a minimum step size of 0.5 dB was reached. The threshold was calculated as the average of the level at six reversals at the minimum step size. The computer monitor displayed a response box with three buttons for the stimulus intervals in a trial. The subject was asked to indicate the interval containing the signal. During stimulus presentation, the buttons in the response box were successively highlighted synchronously with the appropriate interval. The subject responded via the keyboard and received immediate feedback on whether the response was correct or not.

C. Stimuli

1. Intensity discrimination of pure tones and broadband noise

The data on intensity discrimination of a 1 kHz tone and broadband noise were taken from Houtsma *et al.* (1980). The just noticeable level difference was measured as a function of the standard (or reference) level of the tone or noise, which was 20, 30, 40, 50, 60, or 70 dB SPL. The duration of the tone was 800 ms, including 125-ms onset and offset raised-cosine ramps. The noise had a duration of 500 ms, including 50-ms raised-cosine ramps.

2. Tone-in-noise simultaneous masking

Detection thresholds of a 2-kHz signal in the presence of a noise masker were measured for signal durations from 5 to 200 ms, including 2.5-ms raised-cosine ramps. The masker was a Gaussian noise that was band limited to a frequency range from 0.02 to 5 kHz. The masker was presented at a level of 65 dB SPL and had a duration of 500 ms including 10-ms raised-cosine ramps. The signal was temporally centered in the masker.

3. Spectral masking with narrow-band signals and maskers

The data from this experiment were taken from Moore *et al.* (1998). The signal and the masker were either a tone or an 80-Hz wide Gaussian noise. All four signal-masker combinations were considered: tone signal and tone masker (TT),

tone signal and noise masker (TN), noise signal and tone masker (NT), and noise signal and noise masker (NN). In the TT condition, a 90° phase shift between the signal and masker was chosen, while the other conditions used random onset phases of the tone. The masker was centered at 1 kHz, and the signal frequencies were 0.25, 0.5, 0.9, 1.0, 1.1, 2.0, 3.0, and 4.0 kHz. The signal and the masker were presented simultaneously. Both had a duration of 220 ms including 10-ms raised-cosine ramps. Here, only the masker levels of 45 and 85 dB SPLs were considered, whereas the original study also used a level of 65 dB SPL.

4. Forward masking with noise and tone maskers

In the first forward-masking experiment, the masker was a broadband Gaussian noise, band limited to the range from 0.02 to 8 kHz. The steady-state masker duration was 200 ms and 2-ms raised-cosine ramps were applied. Three masker levels were used: 40, 60, and 80 dB SPLs. The signal was a 4-kHz tone. It had a duration of 10 ms and a Hanning window was applied over the entire signal duration. Thresholds were obtained for temporal separations between the masker offset and the signal onset of -20 to 150 ms. For separations between -20 and -10 ms, the signal was presented completely in the masker, i.e., these conditions reflected simultaneous masking.

The second experiment involved forward masking with pure-tone maskers. The stimuli were similar to those used by [Oxenham and Plack \(2000\)](#). Two conditions were used: in the on-frequency condition, the signal and the masker were presented at 4 kHz. In the off-frequency condition, the signal frequency remained at 4 kHz, whereas the masker frequency was 2.4 kHz. The signal was the same as in the first experiment. The signal and the masker had random onset phases in both conditions. The signal level at masked threshold was obtained for several masker levels. In the on-frequency condition, the masker was presented at levels from 30 to 80 dB SPL in 10-dB steps. For the off-frequency condition, the masker was presented at 60, 70, 80, and 85 dB SPLs. The separation between the masker offset and signal onset was either 0 or 30 ms.

5. Modulation detection

The data for the modulation detection experiments were taken from [Dau et al. \(1997a\)](#) for the narrowband-noise carriers and from [Viemeister \(1979\)](#) for the broadband-noise carriers. For the narrowband carriers, a band limited Gaussian noise, centered at 5 kHz, was used as the carrier. The carrier bandwidths were 3, 31, or 314 Hz. The carrier level was 65 dB SPL. The overall duration of the stimuli was 1 s, windowed with 200-ms raised-cosine ramps. Sinusoidal amplitude modulation (SAM) with a frequency in the range from 3 to 100 Hz was applied to the carrier. The duration of the signal modulation was equal to that of the carrier. In the case of the 314-Hz wide carrier, the modulated stimuli were limited to the original (carrier) bandwidth to avoid spectral cues. To eliminate potential level cues, all stimuli were adjusted to have equal power (for details, see [Dau et al., 1997a](#)).

For the broadband-noise carrier, a Gaussian noise with a frequency range from 1 to 6000 Hz was used. The carrier was presented at a level of 77 dB SPL and had a duration of 800 ms. The signal modulation had the same duration and the stimulus was gated with 150-ms raised-cosine ramps, resulting in a 500-ms steady-state portion. Sinusoidal signal modulation, ranging from 4 to 1000 Hz, was imposed on the carrier. There was no level compensation, i.e., the overall level of the modulated stimuli varied slightly depending on the imposed modulation depth.

D. Simulation parameters

The model was calibrated by adjusting the variance of the internal noise so that the model predictions satisfied Weber's law for the intensity discrimination task from Sec. III C 1. When setting up the simulations, the frequency range of the relevant peripheral channels and the suprathreshold signal level for the generation of the template need to be specified. The range of channels was chosen such that potential effects of off-frequency listening were included in the simulations. The on-frequency channel may not always represent the channel with the best signal-to-noise ratio, particularly in the present model where the best frequency of the nonlinear peripheral channels depends on the stimulus level.

The following frequency ranges and suprathreshold signal levels were used in the simulations: For intensity discrimination with tones, the peripheral channels from one octave below to one octave above the signal frequency (1 kHz) were considered. For the broadband noise, all peripheral channels centered from 0.1 to 8 kHz were used. For both experiments, the signal level for the template was chosen to be 5 dB above the standard level. For tone-in-noise masking, the channels from one octave below to one octave above the 2-kHz signal frequency were considered. The signal level for the template was set to 75 dB SPL which is about 10 dB higher than the highest expected masked threshold in the data. For the spectral masking experiments, the channels from half an octave below to one octave above the signal frequency were considered. For the forward-masking experiment with a broadband-noise masker and a 4 kHz signal, the channels from 3.6 to 5 kHz were used. The signal level for the template was chosen to be 10 dB above the masker level. For the forward-masking experiments with pure-tone maskers, only the channel tuned to the signal frequency (4 kHz) was used and the template level was 10 dB above the masker level. In the modulation detection experiment with narrow-band carriers centered at 5 kHz, the channel at 5 kHz was considered as in the study of [Dau et al. \(1997a\)](#) in order to directly compare to the results with the original simulations. For this experiment, the simulations showed a standard deviation that was larger than that in the data. To reduce the standard deviation, simulated thresholds were averages of 20 runs instead of only 3 runs as for all other simulations. For the broadband-noise carrier condition, the channels from 0.1 to 8 kHz were used. In both cases, the modulation depth for the template was chosen to be -6 dB.

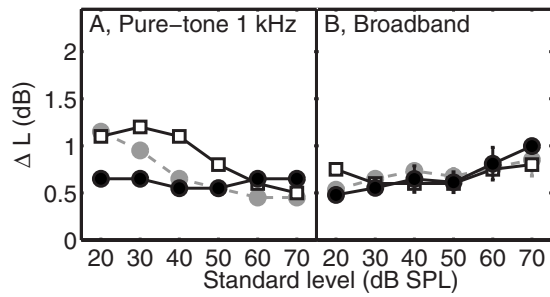


FIG. 3. Intensity discrimination thresholds for a 1-kHz tone (left panel) and broadband noise (right panel) as a function of the standard level. Model predictions (closed symbols) are shown along with measured data (open symbols) taken from Houtsma *et al.* (1980). The gray symbols represent simulations obtained with the model of Dau *et al.* (1997a).

IV. RESULTS

In this section, measured data are compared to simulations. The data are represented by open symbols while simulations are shown as filled symbols. For comparison, gray symbols indicate simulations obtained with the original model. Differences between the predictions of the two models are discussed in more detail in Sec. V.

A. Intensity discrimination

For pure-tone and broadband-noise stimuli, the smallest detectable change in intensity, ΔI , is, to a first approximation, a constant fraction of the standard intensity I of the stimulus (e.g., Miller, 1947). This is referred to as Weber's law. As in many other studies, intensity differences are described in the following as just noticeable differences (JNDs) in level, ΔL .

The broadband-noise JND at medium levels (from 30 to 60 dB) was used to calibrate the model, i.e., to adjust the variance in the internal noise in the model. In the original model, the combination of the logarithmic compression of the stationary parts of the stimuli, realized in the adaptation loops, and the constant-variance internal noise produced a constant Weber fraction (for noise) throughout the entire level range.

Figure 3 shows the JNDs for the 1-kHz tone (panel A) and for broadband noise (panel B)). The simulations (filled circles) are shown together with average data (open squares) taken from Houtsma *et al.* (1980). For the pure tone, the simulated JND is about 0.5 dB for all standard levels considered here. For the levels from 20 to 40 dB SPL, the simulated JNDs lie about 0.5 dB below the data. At higher standard levels, the simulations agree well with the data. The simulation does not reflect the near miss to Weber's law observed in the measured data, i.e., the decrease in threshold with increasing the standard level. This is discussed in detail in Sec. V A. The original model (gray symbols) accounts well for the data at 20 dB SPL and above 50 dB SPL, while the JND for 40 dB SPL lies 0.5 dB below the measured JND.

The measured JNDs for broadband noise (panel B)) are about 0.6 dB for levels from 30 to 50 dB SPL. There is a slight increase at the lowest and the highest levels in the data, resulting in a JND of about 0.8 dB. The simulations agree very well with the data for levels from 30 to 60 dB

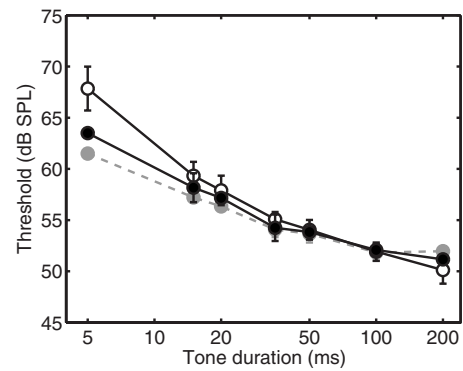


FIG. 4. Results from the tone-in-noise masking experiment with a broadband-noise masker at 65 dB SPL. The signal was a 2-kHz pure tone. The open circles show the mean detection thresholds for the four subjects as a function of signal duration. The error bars indicate one standard deviation. The closed circles indicate the predicted thresholds for the CASP model (black) and the original model (gray).

SPL. For the lowest level (20 dB SPL), the simulated JND lies 0.3 dB below the measured JND, while it is about 0.2 dB above the measured value at the highest level. The simulations obtained with the original model show essentially the same results.

B. Tone-in-noise simultaneous masking

Figure 4 shows the average thresholds of the four listeners from the present study for tone-in-noise masking (open circles). The error bars indicate \pm one standard deviation across subjects, which is typically less than 1 dB but amounts to about 2 dB for the shortest signal duration of 5 ms. For signal durations in the range from 5 to 20 ms, the threshold decreases by about 4–5 dB per doubling of signal duration, while the decrease is about 3 dB per doubling for durations above 20 ms. The data are consistent with results from earlier studies on signal integration in tone-in-noise masking (e.g., Dau *et al.*, 1996b; Oxenham *et al.*, 1997; Oxenham, 1998).

The simulations (filled circles) show a constant decay of 3 dB per doubling of signal duration. This agrees nicely with the measured data for durations at and above 15 ms. At signal durations of 200 ms and above (not shown), the simulations are consistent with the prediction of a threshold of 48 dB obtained with the classical power spectrum model of masking (Patterson and Moore, 1986), assuming a threshold criterion of 1.5 dB increase in power (due to the addition of the signal to the noise) in the passband of the 2 kHz gammatone filter. For the shortest signal duration of 5 ms, the CASP model underestimates the measured threshold by 4 dB. This results from the 3 dB per doubling decay in the simulations observed also for the short durations (5–20 ms) while the data show a somewhat larger slope in this region. The simulations with the original model (gray symbols) show similar results² as the CASP model.

The actual integration of signal information in the model is realized in the optimal detector. The matched-filtering process implies that a variable time constant is available that is matched to the signal duration. The integration of the cross correlator in the detector is similar to the classic notion of

temporal integration, but no fixed integration time constant is necessary for long-term integration. It is the temporal extension of the template which automatically determines the weighting of the stimuli across time. This concept is effectively close to the “multiple-looks” strategy discussed by Viemeister and Wakefield (1991). Time constants that are related to the “hard-wired” part of signal processing within the model represent a lower limit in temporal acuity. The modulation filterbank represents a set of time constants that are, however, too short to account for the long-term integration data. Thus, it is the decision device that inherently accounts for the long effective time constants observed in the present experiment. The result of the decision process depends critically on the properties of the internal representation of the stimuli which forms the input to the detector. The combination of peripheral processing, adaptation, modulation filtering, and decision making, assumed in the present model, leads to good agreement of the predictions with the data in this experimental condition.

C. Spectral masking patterns with narrowband signals and maskers

Masking patterns represent the amount of masking of a signal as a function of signal frequency in the presence of a masker with fixed frequency and level. The shapes of these masking patterns are influenced by several factors, such as occurrence of combination tones or harmonics produced by the peripheral nonlinearities, and by beating cues (Moore and Glasberg, 1987; van der Heijden and Kohlrausch, 1995). Additionally, the width and shape of the masking patterns are level dependent as a consequence of the level-dependent auditory filters. Moore *et al.* (1998) measured masking patterns using pure tones and narrowband noises as signals and pure tones and narrowband noises as maskers for masker levels of 45, 65, and 85 dB SPL. They found that temporal fluctuations (beats) had a strong influence on the measured masking patterns for sinusoidal maskers for masker-signal frequency separations up to a few hundred hertz. The data also indicated some influence of beats for the conditions with narrowband-noise maskers. The simulations obtained with the present model are compared here to the data of Moore *et al.* (1998) and with simulations of Derleth and Dau (2000) using the original model.

The open symbols in Fig. 5 show the mean data of Moore *et al.* (1998). The four panels show the results for conditions TT, TN, NT, and NN. The masking patterns for masker levels of 45 and 85 dB SPL are indicated by squares and circles, respectively. The ordinate represents masking, defined as the difference between the masked threshold and the absolute threshold at each signal frequency. The masking patterns generally show a maximum at the masker frequency. The amount of masking generally decreases with increasing spectral separation between the signal and the masker. For the TT condition, the peak in the masking patterns is particularly pronounced, since beating between the signal and the masker for frequency separations of a few hundred hertz provides a very effective detection cue in this condition (e.g., Moore *et al.*, 1998). The 45 dB SPL masker produces a sym-

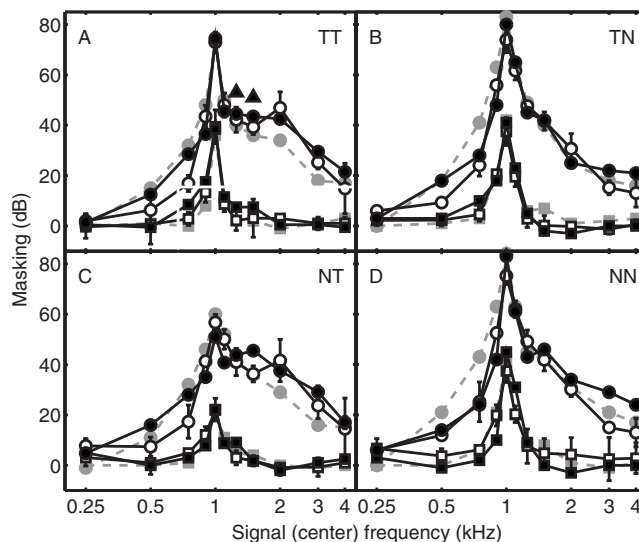


FIG. 5. Spectral masking patterns for the four stimulus conditions. Masking is the difference between the masked and the absolute threshold. The masker was centered at 1 kHz. The squares and circles indicate masker levels of 45 and 85 dB SPL, respectively. The open symbols indicate the measured data (Moore *et al.*, 1998). The closed symbols indicate the simulated patterns. Panel A represents the TT condition. The upward triangles indicate predicted masking where the modulation filters were limited to have a maximum center frequency of 130 Hz. Panels B, C, and D show the patterns in the TN, NT, and NN conditions, respectively. The gray symbols indicate predictions from Derleth and Dau (2000).

metric pattern in all conditions, whereas the pattern for the 85 dB SPL masker is asymmetric with a considerable broadening on the high-frequency side.

The filled symbols in Fig. 5 show the model predictions. In the TT condition, the predictions agree well with the experimental data, except for the signal frequencies of 500 and 750 Hz for the 85 dB SPL masker, where the amount of masking is overestimated. The simulations at this masker level otherwise show the asymmetry found in the measured masking pattern, which in the model is a direct consequence of the level-dependent BM filter shapes. The gray symbols plot the simulated pattern from Derleth and Dau (2000). Using level-invariant, linear gammatone filters, these predictions underestimate the amount of masking at high signal frequencies.

The two filled upward-pointing triangles in panel A indicate simulations that were obtained considering only the first eight modulation filters (with center frequencies ranging up to 130 Hz), while neglecting activity in the remaining modulation filters tuned to modulation rates above 130 Hz. These predictions exceed measured thresholds by up to 15 dB. Within the model, the reason for this deviation from the data is that the beats between the signal and the masker at rates of 150–200 Hz are not represented and cannot contribute to signal detection. Thus, in the framework of the present model, the inclusion of higher-frequency modulation filters between 130 and 250 Hz is crucial to account for the tone-on-tone masking pattern.

The masking patterns for condition TN are shown in panel B. For signal frequencies close to the masker frequency, they are broader than for the TT condition. The sharp peak at 2 kHz that occurred for the tonal masker is not

present for the noise masker. This is also the case in the simulated pattern since the beating cue for small masker-signal frequency separations is less pronounced than in the case of the tonal masker. On the low-frequency side of the masker, the predictions of the CASP model are considerably better than those obtained by [Derleth and Dau \(2000\)](#), where masking was overestimated by up to 18 dB. Thus, as expected, in this condition where energy cues play the most important role, the shapes of the level-dependent BM filters are mainly responsible for the good agreement between the data and the simulations.

Panel C shows the results for condition NT. When the signal and masker are centered at the same frequency, the amount of masking is about 20 dB lower than for the TN and TT conditions. This asymmetry of masking has been reported previously and explained by temporal envelope fluctuations introduced by the noise signal (e.g., [Hellman, 1972](#); [Hall, 1997](#); [Moore et al., 1998](#); [Gockel et al., 2002](#); [Verhey, 2002](#)). The simulated patterns agree very well with the data, except for signal (center) frequencies of 500 and 750 Hz at the high masker level, where masking is overestimated by about 10 dB. Again, the agreement between simulations and data is better for the current model than for the original model which assumed linear BM filters.

Finally, the masking patterns for the NN condition are shown in panel D. The results are similar to those for the TN condition. The simulations agree very well with the measured patterns, except for the signal center frequencies of 3 and 4 kHz, where the masking is overestimated by about 11 dB for the 85 dB masker. The simulations using the original model ([Derleth and Dau, 2000](#), Fig. 4) showed a considerable overestimation of the masking on the low-frequency side of the masker (up to about 20 dB).

In summary, the masking patterns simulated with the CASP model agree well with the measured data in the four masking conditions. For the 45 dB masker, the predictions were similar to those obtained by [Derleth and Dau \(2000\)](#). For the 85 dB masker, however, the simulations were clearly improved as a consequence of the more realistic simulation of level-dependent cochlear frequency selectivity. However, it is the combination of audio-frequency selectivity and the sensitivity to temporal cues, such as beating between the signal and the masker, that is crucial for a successful simulation of masking patterns.

D. Forward masking with noise and on- versus off-frequency tone maskers

The forward-masking experiments of the present study were conducted to test the ability of the CASP model to account for data that have been explained in terms of non-linear cochlear processing. Figure 6 shows the mean masked thresholds for the four subjects (open symbols) for three masker levels (40, 60, 80 dB SPL) as a function of the offset-onset interval between the masker and the signal. The error bars indicate \pm one standard deviation. The mean absolute threshold of the subjects for the brief signal was 12 dB SPL and is indicated in Fig. 6 by the gray horizontal lines. In the simultaneous-masking conditions, represented by the negative offset-onset intervals, the masked thresholds lie slightly

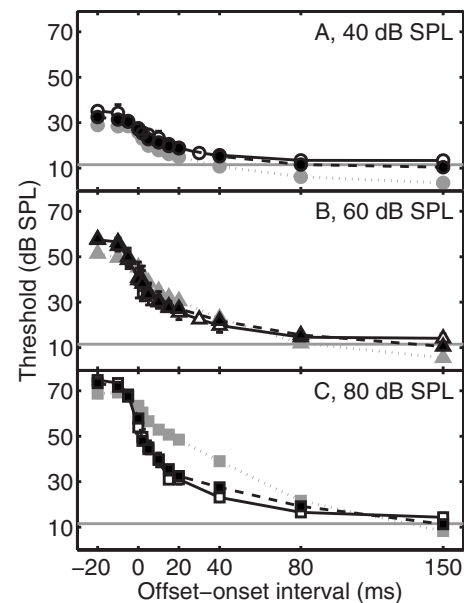


FIG. 6. Forward-masking thresholds obtained with a 10-ms, 4-kHz pure-tone signal and a broadband-noise masker. Results for masker levels of 40, 60, and 80 dB SPLs are indicated in panels A, B, and C, respectively. The open symbols represent the mean data from four subjects, while the closed symbols represent predicted thresholds. Predictions of the original model are given in gray. The abscissa represents the time interval between the masker offset and the signal onset. The horizontal gray lines indicate the absolute threshold of the signal.

below the level of the masker. As expected, the thresholds decrease rapidly for short delays and more slowly for larger delays. At a masker-signal separation of 150 ms, the three forward-masking curves converge near the absolute threshold of the signal.

The simulated forward-masking curves are indicated by the filled symbols in Fig. 6. The model accounts quantitatively for the measured thresholds for all three masker levels. The simulations obtained with the original model (gray symbols) show clear deviations from the data, with a decrease that is too shallow in the 0–40 ms region of the forward-masking curve for the highest masker level (panel C). In the CASP model, peripheral compression influences the thresholds in this region, since the signal level falls in the compressive region around 50 dB SPL. Large changes in the input level are thus required to produce small changes in the internal representation of the signal, resulting in a faster decay of forward masking.

[Oxenham and Plack \(2000\)](#) presented data that demonstrated the role of level-dependent BM processing in forward masking. Similar experiments, using on- and off-frequency pure-tone maskers in forward masking, were conducted here. The hypothesis was that growth of masking (GOM) functions in forward masking should depend on whether the masker and/or the signal level fall within the compressive region of the BM input-output function. If the masker and the signal levels both fall in the compressive region, which is typically the case for very short masker-signal separations, and if the compression slope is assumed to be constant, the signal level at threshold should change linearly with changing masker level by about 1 dB/dB. On the other hand, for larger masker-signal separations, the masker level may fall in

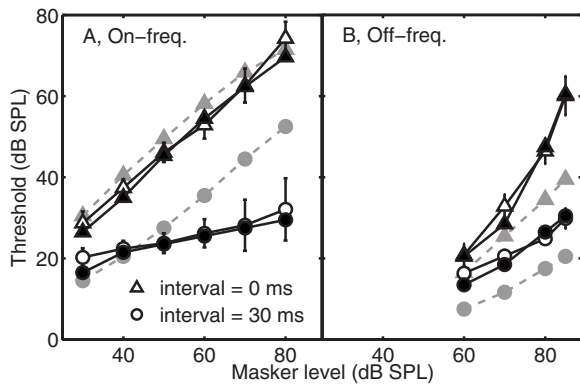


FIG. 7. Panel A shows the GOM curves obtained in the forward-masking experiment, where a 10-ms, 4-kHz pure-tone signal was masked by an on-frequency forward masker. The triangles and circles represent thresholds when the masker-signal interval was 0 and 30 ms, respectively. The open symbols show the mean data of four subjects. The black and gray symbols show simulated thresholds using the CASP and the original model, respectively. In panel B, GOM curves for an off-frequency masker at 2.4 kHz are shown using the same symbols and notation as for panel A.

the compressive region while the signal level falls in the linear region of the BM input-output function. In this case, a given change in masker level will produce a smaller change of the signal level at threshold, leading to a shallower slope of the GOM function. For off-frequency stimulation with a masker frequency well below the signal frequency, the BM response at the signal frequency is assumed to be linear at all levels. The slope of the curves should therefore be roughly independent of the masker-signal interval for off-frequency stimulation. The data presented by Oxenham and Plack (2000) provided evidence for such behavior of the GOM functions by using on- and off-frequency pure-tone maskers.

Figure 7 shows the GOM functions from the second forward-masking experiment of the present study, averaged across the four subjects. Panels A and B show the results for the on- and off-frequency conditions, respectively. Thresholds corresponding to masker-signal intervals of 0 and 30 ms are indicated by triangles and circles, respectively. In the on-frequency condition, the measured slope of the GOM function is close to unity (≈ 0.9 dB/dB) for the 0 ms interval. For the masker-signal interval of 30 ms, the slope of the GOM function is shallower (≈ 0.25 dB/dB). This was expected since the signal and masker can be assumed to be processed in different level regions of the BM input-output function. The data agree with the results of Oxenham and Plack (2000) in terms of the slopes of the GOM functions (0.82 dB/dB for the 0 ms interval and 0.29 dB/dB for the 30 ms interval).

The corresponding simulated GOM functions (filled symbols) for both masker-signal intervals are very close to the measured data. This supports the hypothesis that the non-linear BM stage can account for the different shapes for different intervals. Since the BM stage in the original model processes sound linearly, the slopes of the predicted GOM functions (gray symbols) are similar for the two masker-signal intervals. The failure of the original model to correctly predict the GOM slope for the 30 ms interval was also ob-

served in the first forward-masking experiment for the 30 ms interval for the 80 dB masker from the previous experiment [Fig. 6, Panel C].

For the off-frequency masker, the slope of the GOM function for the 0-ms interval is about 1.2 dB/dB, while it is 0.5 dB/dB for the 30-ms interval. These data are not consistent with the hypothesis that the GOM function for off-frequency stimulation should be independent of the interval. The variability in the average data is very low, with a standard deviation of only 1–2 dB. The data also differ from the average data of Oxenham and Plack (2000, their Fig. 3). They found GOM functions in this condition with a mean slope close to unity for all masker-signal separations. However, there was substantial variability in slope across subjects; some showed a clearly compressive GOM function while other subjects showed a linear or slightly expansive GOM function.

The initial hypothesis was that both the signal and the masker were processed linearly in the off-frequency condition. However, this is not always the case: the signal level can be above 30–40 dB and thus fall in the compressive region of the BM I/O function, while the off-frequency masker is still processed linearly. Such a situation would lead to a GOM function with a slope greater than 1, a trend which is observed in the data in panel B for the 0 ms separation, at least for the two highest masker levels. The data of Oxenham and Plack (2000) for the same interval support this idea, but this was not explicitly discussed in their study.

The simulations for the off-frequency condition closely follow the measured data. The CASP model predicts a GOM function with a slope below 1 for the 30 ms interval, as observed in the data. This is caused by the adaptation stage, which compresses the long-duration off-frequency masker slightly more than the short-duration signal. This slight compression can also be seen in the simulations obtained with the original model (gray circles). For the 0-ms interval, some of the signal thresholds lie in the compressive part (>30 dB SPL) of the BM I/O function (see also Fig. 2A). As a consequence, the GOM function has a slope above 1, since the masker is still processed linearly. The corresponding simulations obtained with the original model show a function which is essentially parallel to the 30 ms function. This model thus fails to account for the different slopes for the two masker-signal intervals.

E. Modulation detection with noise carriers of different bandwidths

In the following, AM detection with random noise carriers of different bandwidths is considered. Figure 8 shows the average data (open symbols) from Dau *et al.* (1997a) for carrier bandwidths of 3, 31, and 314 Hz. Panel (D) shows the “classical” temporal modulation transfer function (TMTF) using a broadband-noise carrier, taken from Viemeister (1979, open symbols). The modulation depth at threshold, in decibels ($20 \log m$), is plotted as a function of the modulation frequency.

The simulations (closed symbols) for the 3-Hz wide carrier account for the main characteristics of the data. The

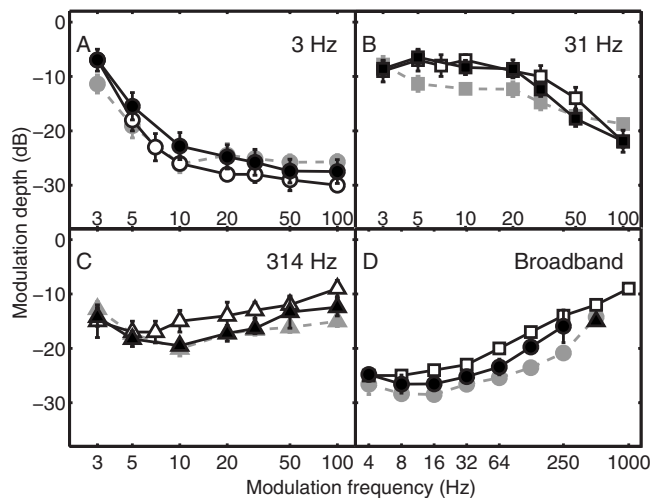


FIG. 8. TMTFs for SAM imposed on noise carriers with different bandwidths. In panels A, B, and C, the measured data of [Dau et al. \(1997a\)](#) are indicated as open symbols for carrier bandwidths of 3, 31, and 314 Hz, respectively. Panel D shows measured data from [Viemeister \(1979\)](#) as open symbols. The black filled symbols represent the simulated TMTFs obtained with the present model. The gray symbols indicate the simulations obtained with the original model. The black triangle indicates the predicted threshold for the 500 Hz modulation frequency when no limiting 150 Hz modulation lowpass filter was used.

simulated TMTF shows a slightly shallower threshold decrease with increasing signal modulation frequency than the measured function. For the 31-Hz wide carrier, the simulated TMTF follows the highpass characteristic observed in the data; only at 50 Hz is the measured threshold underestimated by 3–4 dB. For the 314-Hz wide carrier, the simulated thresholds roughly follow the shape of the measured TMTF, but predicted thresholds are typically 1–3 dB below the data. The agreement of the simulations with the data is slightly worse for the original model than for the present model, except for the 3 Hz bandwidth, where the agreement is similar.

Finally, the broadband TMTF (panel D) shows a low-pass characteristic with a cut-off frequency of about 64 Hz. Thresholds are generally lower than for the 314-Hz wide carrier, which is a consequence of the lower envelope power spectrum density resulting from intrinsic fluctuations in the carrier. Since the envelope spectrum of the carrier extends to the carrier bandwidth, the power density in the envelope spectrum is lower (given that the overall level of the carriers is similar in these two conditions) and stretches over a broader frequency region in the case of the broadband-noise carrier. If the model was based on a broad “predetection” filter instead of a peripheral filterbank, the distribution of power in the envelope spectrum would directly relate to the lower thresholds in the broadband condition. In the model, however, the auditory filters limit the bandwidths of the internal signals and thus the frequency range of their envelope spectra. The lower thresholds obtained with the broadband carriers result from across-frequency integration of modulation information in the model, as shown by [Ewert and Dau \(2000\)](#). The predicted and measured TMTFs have similar shapes for frequencies up to 250 Hz, but the simulated TMTF (closed symbols) lies 1–3 dB below the data. At 500

and 1000 Hz, the modulation is undetectable for the model (even at a modulation depth of 0 dB) and no predicted threshold is shown. This is related to the modulation low-pass filter, which reduces the sensitivity to modulation frequencies above 150 Hz. The filled triangle indicates the simulated threshold for 500 Hz when the limiting lowpass filter was left out. In this case, the result is close to the measured threshold and also similar to the simulated threshold obtained with the original model. However, both the CASP model and the original model fail to predict the measured threshold for the 1000 Hz modulation frequency. It is possible that other cues contribute to detection at these high modulation rates which are not reflected in the modulation filterbank of the present model, such as pitch (e.g., [Burns and Viemeister, 1981](#); [Fitzgerald and Wright, 2005](#)).

V. DISCUSSION

In this section, the effects of the modifications introduced in the CASP model and their interaction with the remaining processing stages are considered. The limitations of the present modeling approach are discussed and potentials for further model investigations addressed.

A. Role of nonlinear cochlear processing in auditory masking

The original model ([Dau et al., 1997a](#)) is quite successful when predicting simultaneous and nonsimultaneous discriminations and masking data, even though the model’s linear processing at the BM level is not realistic. The study of [Derleth et al. \(2001\)](#) demonstrated fundamental problems when trying to implement BM nonlinearity in a straightforward way in the model: when the gammatone filterbank was replaced by a nonlinear cochlear stage, the model could not account for forward masking since the temporal-adaptive properties were substantially affected. One might argue that the assumed processing in the model, particularly the processing in the adaptation stage, is inappropriate since it leads to successful predictions only when combined with a linear BM simulation. However, the simulations obtained with the CASP model demonstrate that forward masking actually can be accounted for including the adaptation stage. One of the reasons for this result is the squaring device that simulates the expansive transformation from inner-hair-cell potentials into AN rate functions. The expansion reduces the amount of (instantaneous) compression introduced by the compressive BM stage while the overall compression in the CASP model is kept level dependent, which is different from the original model. A squaring stage was also included by [Plack et al. \(2002\)](#) in their temporal-window model and was crucial for the success of their model when describing forward masking.

In several of the experimental conditions considered here, the CASP model produced very similar predictions to the original model. In the level discrimination task, the predicted JND in level depends on the overall steady-state compression in the model, which is dominated by the logarithmic compression in the adaptation stage. This leads to a roughly constant discrimination threshold in the model independent of level (see Fig. 3). The level-dependent compression real-

ized in the cochlear processing does not affect the model predictions for broadband noise. For pure tones, the present model predicts slightly lower JNDs than the original model for the lowest standard levels of 20 and 30 dB SPLs.

The original model correctly describes Weber's law within each channel, consistent with intensity discrimination data in notched noise (Viemeister, 1983). With increasing spread of activity into different auditory channels in the multi-channel simulation shown here (Fig. 3, gray symbols), the original model predicts the near miss to Weber's law. The CASP model can no longer predict Weber's law within an individual channel as a consequence of the BM compression at midlevels. An analysis of the model's behavior revealed that, when only a single peripheral channel (centered at the signal frequency) was considered, the pure-tone JNDs were elevated in the midlevel region (50–70 dB SPL) by 0.3–0.4 dB to a maximum of about 1 dB. If a channel tuned to a higher center frequency was analyzed, for which the tone fell in the region of linear processing, the JNDs were level independent. When using an auditory filterbank (as in the simulations shown in Fig. 3), the level-independent JND contributions from the off-frequency channels produce essentially a constant JND across levels, thus minimizing the effect of on-frequency peripheral compression. Thus, the combination of information across frequency leads here to the prediction of Weber's law but does not account for the near miss to Weber's law. This result is consistent with simulations by Heinz *et al.* (2001b) when considering only AN firing rate information (average discharge counts) and disregarding nonlinear phase information. AN fibers with CFs above and below the tone frequency have phase responses that change with level (e.g., Ruggero *et al.*, 1997) and thus contribute information. In their modeling framework, Heinz *et al.* (2001b) showed that the inclusion of nonlinear phase information (at low and moderate CFs where phase information is available) as well as rate-based information can account for the near miss to Weber's law by using an across-frequency coincidence mechanism evaluating this information. Thus, it appears that lack of such an evaluation of nonlinear phase effects across CFs is responsible for the inability of the CASP model to account for the near miss to Weber's law.

The predicted detection of AM is not affected by the amount of cochlear compression in the CASP model, consistent with earlier results of Ewert and Dau (2000) for broadband TMTFs. Since both signal modulation and inherent carrier modulations are compressed in the same way, the signal-to-noise ratio (at the output of the modulation filters) does not change. This is also consistent with the observation that sensorineural hearing-impaired listeners often show about the same sensitivity to modulation independent of the amount of hearing loss (e.g., Bacon and Viemeister, 1985; Formby, 1987; Bacon and Gleitman, 1992) at least for narrow-band noise carriers and for broadband-noise carriers as long as the hearing loss is relatively flat. Accordingly, the characteristics of the spectral masking patterns (as in Fig. 5) that are associated with temporal envelope (beating) cues do not strongly depend on peripheral compression, i.e., the simulations obtained with the present model are very similar

to earlier simulations using the gammatone filterbank. For example, the sharp tuning of the masking pattern for the tone signal and the tone masker and the asymmetry of masking effect for tone-on-noise versus noise-on-tone masking can be accounted for by both models.

However, cochlear nonlinear processing *does* play a crucial role in the other conditions considered in the present study. For the spectral masking patterns obtained with the high masker level (85 dB SPL), the effect of upward spread of masking is accounted for by the level-dependent frequency selectivity in the BM stage, which was not implemented in the original model. In the forward-masking conditions, where the signal and the masker were processed in different regions of the BM input-output function, the results obtained with the CASP model showed much better agreement with the data than the original model. Specifically, in the conditions with an on-frequency tone masker, the measured slopes of the GOM function strongly depend on the masker-signal interval, an effect explained by cochlear compression (Oxenham and Plack, 2000). In the forward-masking condition with the broadband-noise masker, the present model was able to account for the data for all masker levels. In contrast, the original model overestimated forward masking by 15–20 dB for masker-signal intervals of 10–40 ms at the highest masker level (80 dB SPL). These deviations are directly related to the deviations observed in the GOM functions for the tonal masker.

Ewert *et al.* (2007) compared forward-masking simulations from an earlier version of the CASP model to predictions from the temporal-window model (e.g., Oxenham and Moore, 1994; Oxenham, 2001). They investigated whether forward masking was better explained by the concept of neural persistence or temporal integration, as reflected in the temporal-window model, or by the concept of neural adaptation, as reflected in the CASP model. Ewert *et al.* (2007) showed that the two models produce essentially equivalent results and argued that the temporal-window model can be considered a simplified model of adaptation. The reason for the similarity of the two models is that the signal-to-noise ratio based decision criterion at the output of the temporal-window model acts in a way that corresponds to the division process in the adaptation stage of the present model. The remaining difference is that the CASP model includes adaptation effects of the signal itself since the model contains a feedback mechanism in the adaptation loops. In contrast, the temporal-window model only mimics adaptation effects caused by the masker which are modeled using a feed-forward mechanism (Ewert *et al.*, 2007).

B. Effects of other changes in the processing on the overall model performance

The signal transformation through the outer and middle ear was not considered and absolute sensitivity as a function of frequency was only approximated in the original model. In the current model, an outer-ear and a middle-ear transfer functions were implemented. In the experiments considered here, the effect of the absolute threshold was only observed in the forward-masking condition at the largest masker-signal intervals.

The 150-Hz modulation lowpass filter was included in the CASP model to simulate the auditory system's limited sensitivity to high-frequency envelope fluctuations. The filter was chosen based on the results of studies on modulation detection with tonal carriers where performance was limited by internal noise rather than any external statistics of the stimuli. The model accounts well for the broadband-noise TMTF for AM frequencies up to 250 Hz (see Fig. 8). However, the 150-Hz lowpass filter caused predicted thresholds to be too high for high-rate modulations. Additional model predictions for a 500 Hz modulation rate without the 150-Hz filter were very close to those obtained with the original model and the experimental data. This suggests that the slope of the 150 Hz lowpass filter (6 dB/octave) might be too steep. A shallower slope of 3–4 dB/octave would most likely not affect other simulations in the present study substantially while it would still be in line with the modulation detection data for pure-tone carriers of Kohlrausch *et al.* (2000). However, it is also possible that other cues, such as pitch, contribute to the detection of high-frequency modulations. It has been shown that SAM of broadband noise allows melody recognition, even though the pitch strength is weak (e.g., Burns and Viemeister, 1981; Fitzgerald and Wright, 2005). The model does not contain any pitch detection mechanism and is therefore not able to account for potential effects of pitch on AM detection. There might be an additional process responsible for the detection of temporal envelope pitch and (fine-structure) periodicity pitch (Stein *et al.*, 2005). Such a process might already be effective at modulation rates above the lower limit of pitch (of about 30 Hz) but particularly at high modulation rates (above about 200 Hz) which are not represented or are strongly attenuated in the internal representation of the stimuli in the CASP model.

Another modification of the original model was that the center frequencies of the modulation filters were restricted to one-quarter of the center frequency of the corresponding peripheral channel but never exceeded 1 kHz. In the spectral masking experiment of the present study, with a masker centered at 1 kHz, the simulations showed very good agreement with the data, suggesting that beating cues up to about 250 Hz can contribute to signal detection, at least in the high-level masker condition. However, it is difficult to determine the upper limit of the “existence region” of modulation filters since the sidebands are typically either spectrally resolved by the auditory filters (for tonal carriers) or the modulation depth required for detection is very large (for broadband-noise carriers) such that there is not enough dynamic range available to accurately estimate any meaningful modulation filter characteristic (Ewert and Dau, 2000; Ewert *et al.*, 2002). The combination of the first-order 150 Hz modulation lowpass filter (that provides the “absolute” threshold for AM detection) and the modulation bandpass filtering (over a modulation frequency range that scales with the carrier or “audio” frequency) appears to be successful in various experimental conditions.

C. Limitations of the model

Several studies of modulation depth discrimination (e.g., Wakefield and Viemeister, 1990; Lee and Bacon, 1997; Ewert and Dau, 2004) showed that Weber's law holds for most modulation depths, i.e., the JND of AM depth is proportional to the reference modulation depth. A modified internal-noise source would be required in the model to account for these data (Ewert and Dau, 2004). Such a noise could be modeled either by a multiplicative internal noise at the output of the modulation filters or by a logarithmic compression of the rms output of the modulation filter (see Ewert and Dau, 2004). Neither the original model nor the CASP model can predict Weber's law in this task since a level-independent fixed-variance internal noise is assumed. As described earlier, both models do account for Weber's law in intensity discrimination since the preprocessing realizes a logarithmic compression for stationary signals (due to the adaptation stage). However, the AM depth for input fluctuations with rates higher than 2 Hz (which are represented in the modulation bandpass filters) is transformed almost linearly by the adaptation stage. Thus, the CASP model fails in these conditions. This might be improved by including an additional nonlinearity in the modulation domain. Such a modification was considered to be beyond the scope of the present study.

Shamma and co-workers (e.g., Chi *et al.*, 1999; Elhilali *et al.*, 2003) described a model that is conceptually similar to the CASP model but includes an additional “dimension” in the signal analysis. They suggested a spectrotemporal analysis of the envelope, motivated by neurophysiological findings in the auditory cortex (Schreiner and Calhoun, 1995; de Charms *et al.*, 1998). In their model, a “spectral” modulation filterbank was combined with the temporal modulation analysis, resulting in two-dimensional spectrotemporal filters. Thus, in contrast to the implementation presented here, their model contains joint (and inseparable) spectro-temporal modulations. In conditions where both temporal and spectral features of the input are manipulated, the two models respond differently. The model of Shamma and co-workers has been utilized to account for spectrotemporal modulation transfer functions for the assessment of speech intelligibility (Chi *et al.*, 1999; Elhilali *et al.*, 2003), the prediction of musical timbre (Ru and Shamma, 1997), and the perception of certain complex sounds (Carlyon and Shamma, 2003). The CASP model is sensitive to spectral envelope modulation which is reflected as a variation in the energy (considered at the output of the modulation lowpass filter) as a function of the audio-frequency (peripheral) channel. For temporal modulation frequencies below 10 Hz, where the phase of the envelope is preserved, the present model could thus use spectrotemporal modulations as a detection cue. The main difference to the model of Chi *et al.* (1999), however, is that the CASP model does not include joint spectrotemporal channels. It is not clear to the authors of the present study to what extent detection or masking experiments can assess the existence of joint spectrotemporal modulation filters. The assumption of the CASP model that (temporal) modulations are processed independently at the output of each auditory

filter implies that across-channel modulation processing cannot be accounted for. This reflects a limitation of the CASP model.

D. Perspectives

Recently, comodulation masking release (CMR) has been modeled using an equalization-cancellation (EC) mechanism for the processing of activity across audio frequencies (Piechowiak *et al.*, 2007). The EC process was assumed to take place at the output of the modulation filterbank for each audio-frequency channel. In that model, linear BM filtering was assumed. The model developed in the present study will allow a quantitative investigation of the effects of nonlinear BM processing, specifically the influence of level-dependent frequency selectivity, compression, and suppression, on CMR. The model might be valuable when simulating the numerous experimental data that have been described in the literature and might, in particular, help in interpreting the role of within- versus across-channel contributions to CMR.

Another challenge will be to extend the model to binaural processing. The model of Breebaart *et al.* (2001a, 2001b, 2001c) accounted for certain effects of binaural signal detection, while their monaural preprocessing was based on the model of Dau *et al.* (1996a), i.e., without BM nonlinearity and without the assumption of a modulation filterbank. Effects of BM compression (Breebaart *et al.*, 2001a, 2001b, 2001c) and the role of modulation frequency selectivity (Thompson and Dau, 2008) in binaural detection have been discussed but not yet considered in a common modeling framework.

An important perspective of the CASP model is the modeling of hearing loss and its consequences for perception. This may be possible because the model now includes realistic cochlear compression and level-dependent cochlear tuning. Cochlear hearing loss is often associated with lost or reduced compression (Moore, 1995). Lopez-Poveda and Meddis (2001) suggested how to reduce the amount of compression in the DRNL to simulate loss of outer hair cells for moderate and severe hearing loss. This could be used in the present modeling framework as a basis for predicting the outcome of a large variety of psychoacoustic tasks in (sensorineural) hearing-impaired listeners.

VI. SUMMARY

The CASP model was developed, representing a major modification in the original modulation filterbank model of Dau *et al.* (1997a). The CASP model includes an outer- and a middle-ear transformation and a nonlinear cochlear filtering stage, the DRNL, that replaces the linear gammatone filterbank used in the original model. A squaring expansion was included before the adaptation stage and a modulation lowpass filter at 150 Hz was used prior to the modulation bandpass filterbank. The adaptation stage, the main parameters of the modulation filterbank, and the optimal detector were the same as in the original model.

Model simulations were compared to data for intensity discrimination with tones and broadband noise, tone-in-noise

TABLE I. The left column shows the original values of the DRNL filterbank parameters which were changed in the present study to reduce the filter bandwidths and the amount of compression at BFs higher than 1.5 kHz. The right column shows the values used in the CASP model.

Parameter	Original		Present	
	p_0	m	p_0	m
BW_{lin}	0.037 28	0.785 63	0.037 28	0.75
BW_{nlin}	-0.031 93	0.774 26	-0.031 93	0.77
$LP_{lin\ cutoff}$	-0.067 62	1.016 73	-0.067 62	1.01
$a_{CF>1.5\ kHz}$	1.402 98	0.819 16	4.004 71	0.00
$b_{CF>1.5\ kHz}$	1.619 12	-0.818 67	-0.980 15	0.00

detection as a function of tone duration, spectral masking with tonal and narrow-band-noise signals and maskers, forward masking with tone signals and (on- and off-frequency) noise and tone maskers, and AM detection using narrow-band and wideband noise carriers.

The model was shown to account well for most aspects of the data. In some cases (intensity discrimination, signal integration in noise, AM detection), the simulation results were similar to those for the original model. In other cases (forward masking with noise and tone maskers, spectral masking at high masker levels), the CASP model showed much better agreement with the data than the original model, mainly as a consequence of the level-dependent compression and frequency selectivity in the cochlear processing.

ACKNOWLEDGMENTS

This work was supported by the Danish Research Foundation, the Danish Graduate school SNAK (“Sense organs, neural networks, behavior, and communication”), the Oticon Foundation, and the Deutsche Forschungsgemeinschaft (DFG, SFB/TRR 31). The authors would like to thank Brian C. J. Moore and two anonymous reviewers for their very helpful and supportive comments.

APPENDIX: DRNL PARAMETERS OF THE MODEL

The parameters of the human DRNL filterbank used in the CASP model were slightly different from those by Lopez-Poveda and Meddis (2001, Table III, average response). Table I shows the original parameters (Lopez-Poveda and Meddis, 2001, left column) and the parameters used here (right column). They were calculated from regression-line coefficients of the form $\log_{10}(\text{parameter}) = p_0 + m \log_{10}(\text{BF})$, where BF is expressed in Hz. Parameters a and b are the same as the original for BFs below 1.5 kHz. For larger BFs, they are set to be constant to reduce the amount of compression. The original value of the compression exponent c was 0.25 and is unchanged. The amount of compression is not determined by c alone, but by a combination of parameters a , b , and c as a consequence of the parallel processing structure of the DRNL algorithm.

¹MATLAB implementations of the model stages are available under the name “Computational Auditory Signal-processing and Perception (CASP) model” on our laboratory’s website: <http://www.dtu.dk/centre/cahr/>

downloads.aspx. Implementations of stages from earlier papers are also included, e.g., Dau *et al.* (1996a, 1997a).

²The same condition was earlier tested using the model described by Dau *et al.* (1996a). The model produced a much too shallow decay of the threshold function with increasing signal duration. This was mainly caused by the excessive overshoot produced by the adaptation stage in response to the signal onset, such that information from the steady-state portion of the signal hardly contributed to the detection of the signal. The onset response of the adaptation stage was therefore limited in the study of Dau *et al.* (1997a) in order to obtain a more realistic ratio of onset and steady-state amplitude.

- Bacon, S. P., and Gleitman, R. M. (1992). "Modulation detection in subjects with relatively flat hearing losses," *J. Speech Hear. Res.* **35**, 642–653.
- Bacon, S. P., and Grantham, D. W. (1989). "Modulation masking: Effects of modulation frequency, depth and phase," *J. Acoust. Soc. Am.* **85**, 2575–2580.
- Bacon, S. P., and Viemeister, N. F. (1985). "Temporal modulation transfer functions in normal-hearing and hearing-impaired listeners," *Audiology* **24**, 117–134.
- Breebaart, J., van de Par, S., and Kohlrausch, A. (2001a). "Binaural processing model based on contralateral inhibition. I. Model structure," *J. Acoust. Soc. Am.* **110**, 1074–1088.
- Breebaart, J., van de Par, S., and Kohlrausch, A. (2001b). "Binaural processing model based on contralateral inhibition. II. Dependence on spectral parameters," *J. Acoust. Soc. Am.* **110**, 1089–1104.
- Breebaart, J., van de Par, S., and Kohlrausch, A. (2001c). "Binaural processing model based on contralateral inhibition. III. Dependence on temporal parameter," *J. Acoust. Soc. Am.* **110**, 1105–1117.
- Bruce, I. C., Sachs, M. B., and Young, E. D. (2003). "An auditory-periphery model of the effects of acoustic trauma on auditory nerve responses," *J. Acoust. Soc. Am.* **113**, 369–388.
- Buchholz, J. M., and Mourjoulous, J. (2004a). "A computational auditory masking model based on signal dependent compression. I. Model description and performance analysis," *Acust. Acta Acust.* **5**, 873–886.
- Buchholz, J. M., and Mourjoulous, J. (2004b). "A computational auditory masking model based on signal dependent compression. II. Model simulations and analytical approximations," *Acust. Acta Acust.* **5**, 887–900.
- Burns, E. M., and Viemeister, N. F. (1981). "Played-again SAM: Further observations on the pitch of amplitude-modulated noise," *J. Acoust. Soc. Am.* **70**, 1655–1660.
- Carlyon, R. P., and Shamma, S. (2003). "An account of monaural phase sensitivity," *J. Acoust. Soc. Am.* **114**, 333–348.
- Carney, L. H. (1993). "A model for the responses of low-frequency auditory-nerve fibers in cat," *J. Acoust. Soc. Am.* **93**, 401–417.
- Chi, T., Gao, Y., Guyton, M. C., Ru, P., and Shamma, S. (1999). "Spectro-temporal modulation transfer functions and speech intelligibility," *J. Acoust. Soc. Am.* **106**, 2719–2732.
- Colburn, H. S., Carney, L. H., and Heinz, M. G. (2003). "Quantifying the information in auditory-nerve responses for level discrimination," *J. Assoc. Res. Otolaryngol.* **4**, 294–311.
- Dau, T., Püschel, D., and Kohlrausch, A. (1996a). "A quantitative model of the effective signal processing in the auditory system. I. Model structure," *J. Acoust. Soc. Am.* **99**, 3615–3622.
- Dau, T., Püschel, D., and Kohlrausch, A. (1996b). "A quantitative model of the effective signal processing in the auditory system. II. Simulations and measurements," *J. Acoust. Soc. Am.* **99**, 3623–3631.
- Dau, T., Kollmeier, B., and Kohlrausch, A. (1997a). "Modeling auditory processing of amplitude modulation. I. Detection and masking with narrow-band carriers," *J. Acoust. Soc. Am.* **102**, 2892–2905.
- Dau, T., Kollmeier, B., and Kohlrausch, A. (1997b). "Modeling auditory processing of amplitude modulation. II. Spectral and temporal integration," *J. Acoust. Soc. Am.* **102**, 2906–2919.
- de Charms, R. C., Blake, D. T., and Merzenich, M. M. (1998). "Optimizing sound features for cortical neurons," *Science* **280**, 1439–1443.
- Derleth, R. P., and Dau, T. (2000). "On the role of envelope fluctuation processing in spectral masking," *J. Acoust. Soc. Am.* **108**, 285–296.
- Derleth, R. P., Dau, T., and Kollmeier, B. (2001). "Modeling temporal and compressive properties of the normal and impaired auditory system," *Hear. Res.* **159**, 132–149.
- Dicke, U., Ewert, S. D., Dau, T., and Kollmeier, B. (2007). "A neural circuit transforming temporal periodicity information into a rate-based representation in the mammalian auditory system," *J. Acoust. Soc. Am.* **121**, 310–326.
- Elhilali, M., Chi, T., and Shamma, S. (2003). "A spectro-temporal modulation index (STMI) for assessment of speech intelligibility," *Speech Commun.* **41**, 331–348.
- Ewert, S. D., and Dau, T. (2000). "Characterizing frequency selectivity for envelope fluctuations," *J. Acoust. Soc. Am.* **108**, 1181–1196.
- Ewert, S. D., and Dau, T. (2004). "External and internal limitations in amplitude-modulation processing," *J. Acoust. Soc. Am.* **116**, 478–490.
- Ewert, S. D., Verhey, J. L., and Dau, T. (2002). "Spectro-temporal processing in the envelope-frequency domain," *J. Acoust. Soc. Am.* **112**, 2921–2931.
- Ewert, S. D., Hau, O., and Dau, T. (2007). "Forward masking: Temporal integration or adaptation?," in *Hearing—From Sensory Processing to Perception*, edited by B. Kollmeier, G. Klump, V. Hohmann, U. Langemann, M. Mauermann, S. Uppenkamp, and J. Verhey (Springer-Verlag, Berlin), pp. 165–174.
- Fitzgerald, M. B., and Wright, B. A. (2005). "A perceptual learning investigation of the pitch elicited by amplitude-modulated noise," *J. Acoust. Soc. Am.* **118**, 3794–3803.
- Formby, C. C. (1987). "Modulation threshold functions for chronically impaired Ménière patients," *Audiology* **26**, 89–102.
- Glasberg, B. R., and Moore, B. C. J. (1990). "Derivation of auditory filter shapes from notched-noise data," *Hear. Res.* **47**, 103–138.
- Gockel, H., Moore, B. C. J., and Patterson, R. D. (2002). "Asymmetry of masking between complex tones and noise: The role of temporal structure and peripheral compression," *J. Acoust. Soc. Am.* **111**, 2759–2770.
- Goode, R. L., Killion, M. L., Nakamura, K., and Nishihara, S. (1994). "New knowledge about the function of the human middle ear: Development of an improved analogue model," *Am. J. Otol.* **15**, 145–154.
- Green, D. M., and Swets, J. (1966). *Signal Detection Theory and Psychophysics* (Wiley, New York).
- Hall, J. L. (1997). "Asymmetry of masking revisited: Generalization of masker and probe bandwidth," *J. Acoust. Soc. Am.* **101**, 1023–1033.
- Hansen, M., and Kollmeier, B. (1999). "Continuous assessment of time-varying speech quality," *J. Acoust. Soc. Am.* **106**, 2888–2899.
- Hansen, M., and Kollmeier, B. (2000). "Objective modeling of speech quality with a psychoacoustically validated auditory model," *J. Audio Eng. Soc.* **48**, 395–409.
- Heinz, M. G., Colburn, H. S., and Carney, L. H. (2001a). "Evaluating auditory performance limits: I. One-parameter discrimination using a computational model for the auditory nerve," *Neural Comput.* **13**, 2273–2316.
- Heinz, M. G., Colburn, H. S., and Carney, L. H. (2001b). "Rate and timing cues associated with the cochlear amplifier: Level discrimination based on monaural cross-frequency coincidence detection," *J. Acoust. Soc. Am.* **100**, 2065–2084.
- Hellman, R. P. (1972). "Asymmetry of masking between noise and tone," *Percept. Psychophys.* **11**, 241–246.
- Hewitt, M. J., and Meddis, R. (1994). "A computer model of amplitude-modulation sensitivity of single units in the inferior colliculus," *J. Acoust. Soc. Am.* **95**, 2145–2159.
- Holube, I., and Kollmeier, B. (1996). "Speech intelligibility prediction in hearing-impaired listeners based on a psychoacoustically motivated perception model," *J. Acoust. Soc. Am.* **100**, 1703–1716.
- Houtgast, T. (1989). "Frequency selectivity in amplitude-modulation detection," *J. Acoust. Soc. Am.* **85**, 1676–1680.
- Houtsma, A. J. M., Durlach, N. I., and Braida, L. D. (1980). "Intensity perception. XI. Experimental results on the relation of intensity resolution to loudness matching," *J. Acoust. Soc. Am.* **68**, 807–813.
- Huber, R., and Kollmeier, B. (2006). "PEMO-Q—a new method for objective audio quality assessment using a model of auditory perception," *IEEE Trans. Audio, Speech, Lang. Process.* **14**, 1902–1911.
- Irino, T., and Patterson, R. D. (2006). "Dynamic, compressive Gammachirp Auditory Filterbank for Perceptual Signal Processing," *International Conference on Acoustics, Speech and Signal Processing, Proc. IEEE* **5**, 133–136.
- Jesteadt, W., Bacon, S. P., and Lehman, J. R. (1982). "Forward masking as a function of frequency, masker level, and signal delay," *J. Acoust. Soc. Am.* **71**, 950–962.
- Kohlrausch, A., Fassel, R., and Dau, T. (2000). "The influence of carrier level and frequency on modulation and beat-detection thresholds for sinusoidal carriers," *J. Acoust. Soc. Am.* **108**, 723–734.
- Langner, G. (1981). "Neuronal mechanisms for pitch analysis in the time domain," *Exp. Brain Res.* **44**, 450–454.
- Langner, G. (1992). "Periodicity coding in the auditory system," *Hear. Res.* **60**, 115–142.

- Langner, G., and Schreiner, C. (1988). "Periodicity coding in the inferior colliculus of the cat. I. Neuronal mechanism," *J. Neurophysiol.* **60**, 1799–1822.
- Lee, J., and Bacon, S. P. (1997). "Amplitude modulation depth discrimination of a sinusoidal carrier: Effect of stimulus duration," *J. Acoust. Soc. Am.* **101**, 3688–3693.
- Lopez-Poveda, E. A., and Meddis, R. (2001). "A human nonlinear cochlear filterbank," *J. Acoust. Soc. Am.* **110**, 3107–3118.
- Lopez-Poveda, E. A., Plack, C. J., and Meddis, R. (2003). "Cochlear non-linearity between 500 and 8000 Hz in listeners with normal hearing," *J. Acoust. Soc. Am.* **113**, 951–960.
- Meddis, R., and O'Mard, L. P. (2005). "A computer model of the auditory-nerve response to forward-masking stimuli," *J. Acoust. Soc. Am.* **117**, 3787–3798.
- Meddis, R., O'Mard, L. P., and Lopez-Poveda, E. A. (2001). "A computational algorithm for computing nonlinear auditory frequency selectivity," *J. Acoust. Soc. Am.* **109**, 2852–2861.
- Miller, G. A. (1947). "Sensitivity to changes in the intensity of white noise and its relation to masking and loudness," *J. Acoust. Soc. Am.* **19**, 609–619.
- Moore, B. C. J. (1995). *Perceptual Consequences of Cochlear Damage* (Oxford University Press, New York).
- Moore, B. C. J., Alcantara, J. I., and Dau, T. (1998). "Masking patterns for sinusoidal and narrow-band noise maskers," *J. Acoust. Soc. Am.* **104**, 1023–1038.
- Moore, B. C. J., and Glasberg, B. R. (1987). "Factors affecting thresholds for sinusoidal signals in narrow-band maskers with fluctuating envelopes," *J. Acoust. Soc. Am.* **82**, 69–79.
- Moore, B. C. J., and Glasberg, B. R. (2003). "Behavioural measurement of level-dependent shifts in the vibration pattern on the basilar membrane at 1 and 2 kHz," *Hear. Res.* **175**, 66–74.
- Moore, B. C. J., Glasberg, B. R., Plack, C. J., and Biswas, A. K. (1988). "The shape of the ear's temporal window," *J. Acoust. Soc. Am.* **83**, 1102–1116.
- Muller, M., Robertson, D., and Yates, G. K. (1991). "Rate-versus-level functions of primary auditory nerve fibres: Evidence for square law behaviour of all fibre categories in the guinea pig," *Hear. Res.* **55**, 50–56.
- Nelson, D. A., and Swain, A. (1996). "Temporal resolution within the upper accessory excitation of a masker," *Acust. Acta Acust.* **82**, 328–334.
- Nelson, P. C., and Carney, L. H. (2004). "A phenomenological model of peripheral and central neural responses to amplitude-modulated tones," *J. Acoust. Soc. Am.* **116**, 2173–2186.
- Oxenham, A. J. (1998). "Temporal integration at 6 kHz as a function of masker bandwidth," *J. Acoust. Soc. Am.* **103**, 1033–1042.
- Oxenham, A. J. (2001). "Forward masking: Adaptation or integration?," *J. Acoust. Soc. Am.* **109**, 732–741.
- Oxenham, A. J., and Moore, B. C. J. (1994). "Modeling the additivity of nonsimultaneous masking," *Hear. Res.* **80**, 105–118.
- Oxenham, A. J., Moore, B. C. J., and Vickers, D. A. (1997). "Short-term temporal integration: Evidence for the influence of peripheral compression," *J. Acoust. Soc. Am.* **101**, 3676–3687.
- Oxenham, A. J., and Plack, C. J. (2000). "Effects of masker frequency and duration in forward masking: Further evidence for the influence of peripheral nonlinearity," *Hear. Res.* **150**, 258–266.
- Palmer, A. R. (1995). "Neural signal processing," in *Hearing*, edited by B. C. J. Moore (Academic, New York).
- Palmer, A. R., and Russell, I. J. (1986). "Phase locking in the cochlear nerve of the guinea-pig and its relation to the receptor potential of inner hair-cells," *Hear. Res.* **24**, 1–15.
- Patterson, R. D., Allerhand, M. H., and Giguere, C. (1995). "Time-domain modeling of peripheral auditory processing: A modular architecture and a software platform," *J. Acoust. Soc. Am.* **98**, 1890–1894.
- Patterson, R. D., and Moore, B. C. J. (1986). "Auditory filters and excitation patterns as representations of frequency resolution," in *Frequency Selectivity in Hearing* (Academic Press, London).
- Piechowiak, T., Ewert, S. D., and Dau, T. (2007). "Modeling comodulation masking release using an equalization-cancellation mechanism," *J. Acoust. Soc. Am.* **121**, 2111–2126.
- Plack, C. J., and Oxenham, A. J. (1998). "Basilar-membrane nonlinearity and the growth of forward masking," *J. Acoust. Soc. Am.* **103**, 1598–1608.
- Plack, C. J., and Oxenham, A. J. (2000). "Basilar-membrane nonlinearity estimated by pulsation threshold," *J. Acoust. Soc. Am.* **107**, 501–507.
- Plack, C. J., Oxenham, A. J., and Drga, V. (2002). "Linear and nonlinear processes in temporal masking," *Acust. Acta Acust.* **88**, 348–358.
- Plasberg, J. H., and Kleijn, W. B. (2007). "The sensitivity matrix: Using advanced auditory models in speech and audio processing," *IEEE Trans. Audio, Speech, Lang. Process.* **15**, 310–319.
- Pralong, D., and Carlile, S. (1996). "The role of individualized headphone calibration for the generation of high fidelity virtual auditory space," *J. Acoust. Soc. Am.* **100**, 3785–3793.
- Püschel, D. (1988). "Prinzipien der zeitlichen Analyse beim Hören," (Principles of Temporal Processing in Hearing), Ph.D. thesis, University of Göttingen.
- Rosengard, P. S., Oxenham, A. J., and Braida, L. D. (2005). "Comparing different estimates of cochlear compression in listeners with normal and impaired hearing," *J. Acoust. Soc. Am.* **117**, 3028–3041.
- Ru, P., and Shamma, S. A. (1997). "Representation of musical timbre in the auditory cortex," *J. New Music Res.* **26**, 154–169.
- Ruggero, M. A., and Rich, N. C. (1991). "Furosemide alters organ of corti mechanics: Evidence for feedback of outer haircells upon the basilar membrane," *J. Neurosci.* **11**, 1057–1067.
- Ruggero, M. A., Rich, N. C., Recio, A., Narayan, S. S., and Robles, L. (1997). "Basilar-membrane responses to tones at the base of the chinchilla cochlea," *J. Acoust. Soc. Am.* **101**, 2151–2163.
- Schreiner, C. E., and Calhoun, B. (1995). "Spectral envelope coding in cat primary auditory cortex: Properties of ripple transfer functions," *Aud. Neurosci.* **1**, 39–61.
- Schroeder, M. R., and Hall, J. L. (1974). "Model for mechanical to neural transduction in the auditory receptor," *J. Acoust. Soc. Am.* **55**, 1055–1060.
- Siebert, W. M. (1965). "Some implications of the stochastic behavior of primary auditory neurons," *Kybernetik* **2**, 206–215.
- Siebert, W. M. (1968). MIT Research Laboratory of Electronics Quarterly Report No. 88.
- Siebert, W. M. (1970). "Frequency discrimination in the auditory system: Place or periodicity mechanism," *Proc. IEEE* **58**, 723–730.
- Smith, R. L. (1977). "Short-term adaptation in single auditory-nerve fibers: Some post-stimulatory effects," *J. Neurophysiol.* **49**, 1098–1112.
- Stein, A., Ewert, D. S., and Wiegand, L. (2005). "Perceptual interaction between carrier periodicity and amplitude modulation in broadband stimuli: A comparison of the autocorrelation and modulation-filterbank model," *J. Acoust. Soc. Am.* **118**, 2470–2481.
- Strube, H. W. (1985). "Computationally efficient basilar-membrane model," *Acustica* **58**, 207–214.
- Tchorz, J., and Kollmeier, B. (1999). "A model of auditory perception as front end for automatic speech recognition," *J. Acoust. Soc. Am.* **106**, 2040–2050.
- Thompson, E., and Dau, T. (2008). "Binaural processing of modulated interaural level differences," *J. Acoust. Soc. Am.* **123**, 1017–1029.
- van der Heijden, M., and Kohlrausch, A. (1995). "The role of envelope fluctuations in spectral masking," *J. Acoust. Soc. Am.* **97**, 1800–1807.
- Verhey, J. L. (2002). "Modeling the influence of inherent envelope fluctuations in simultaneous masking experiments," *J. Acoust. Soc. Am.* **111**, 1018–1025.
- Verhey, J. L., Dau, T., and Kollmeier, B. (1999). "Within-channel cues in comodulation masking release (CMR): Experiments and model predictions using a modulation-filterbank model," *J. Acoust. Soc. Am.* **106**, 2733–2745.
- Viemeister, N., and Wakefield, G. (1991). "Temporal integration and multiple looks," *J. Acoust. Soc. Am.* **90**, 858–865.
- Viemeister, N. F. (1979). "Temporal modulation transfer functions based upon modulation thresholds," *J. Acoust. Soc. Am.* **66**, 1364–1380.
- Viemeister, N. F. (1983). "Auditory intensity discrimination at high frequencies in the presence of noise," *Science* **221**, 1206–1208.
- Wakefield, G. H., and Viemeister, N. F. (1990). "Discrimination of modulation depth of sinusoidal amplitude modulation (SAM) noise," *J. Acoust. Soc. Am.* **88**, 1367–1373.
- Westermann, L. A., and Smith, R. L. (1984). "Rapid and short-term adaptation in auditory nerve responses," *Hear. Res.* **15**, 249–260.
- Yates, G. K., Winter, I. M., and Robertson, D. (1990). "Basilar membrane nonlinearity determines auditory nerve rate-intensity functions and cochlear dynamic range," *Hear. Res.* **45**, 203–220.
- Zhang, X., Heinz, M. G., Bruce, I. C., and Carney, L. H. (2001). "A phenomenological model for the responses of auditory-nerve fibers. I. Non-linear tuning with compression and suppression," *J. Acoust. Soc. Am.* **109**, 648–670.